Langmuir

Article

pubs.acs.org/Langmuir

Electrochemical Properties of Metal-Oxide-Coated Carbon Electrodes Prepared by Atomic Layer Deposition

James A. Loussaert, Stephen E. Fosdick, and Richard M. Crooks*

Department of Chemistry, Center for Electrochemistry, and the Center for Nano- and Molecular Science and Technology, The University of Texas at Austin, 105 E. 24th St., Stop A5300, Austin, Texas 78712-1224, United States

Supporting Information

ABSTRACT: Here we report on the electrochemical properties of carbon electrodes coated with thin layers of Al_2O_3 and SnO_2. These oxide films were deposited using atomic layer deposition (ALD) and range in thickness from 1 to 6 nm. Electrochemical experiments show that the thinnest oxide layers contain defects that penetrate to the underlying carbon electrode. However, oxygenation of the carbon surface prior to ALD increases the surface concentration of nucleation sites for oxide growth and suppresses the defect density. Films of Al_2O_3 just ~3−4 nm in thickness are free of pinholes. Slightly thicker coatings of SnO_2 are required for equivalent passivation. Both Al_2O_3 and SnO_2 films are stable in both neutral and acidic electrolytes even after repeated voltammetric scanning. The results reported here open up the possibility of studying the effect of oxide supports on electrocatalytic reactions.

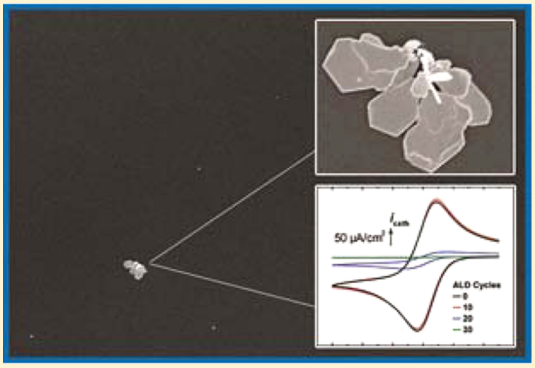

INTRODUCTION

In this paper we report on the impact of thin metal oxide layers, prepared by atomic layer deposition (ALD),[1−4] on a representative electrode material (carbon) and specifically how these oxide layers affect electron-transfer to redox molecules in solution. The results form a basis for our future studies aimed at understanding how oxide supports affect electrocatalytic reactions. Accordingly, we discuss optimal procedures for fabricating and characterizing pyrolyzed photoresist film (PPF)[5,6] electrodes modified with thin ALD layers of Al_2O_3 and SnO_2 and the effect of deposition parameters on the thickness, defect density, and stability of these composite electrodes.[7]

Vapor-phase, layer-by-layer deposition is generally divided into two categories: molecular-layer deposition and ALD.[8−12] We focus here exclusively on ALD, which is a process wherein layers of metal oxides,[1,2] nitrides,[1,13] and zerovalent metal films are formed iteratively on an appropriate solid support.[14,15] The process for depositing a metal oxide begins by introducing a metal precursor, such as those used here, trimethylaluminum (TMA) or tetrakis(dimethylamino)tin(IV) (TDMASn), to a hydroxylated surface at low pressure (<1 mmHg). These precursors react spontaneously with surface-confined hydroxyl groups leading to immobilization of a monolayer or submonolayer of the metal. Next, unreacted precursor and byproducts are removed from the reaction chamber in a purge step. Finally, an oxygen source, such as H_2O, H_2O_2, or O_3, is introduced to form a new layer of hydroxyl groups on the metal surface.[1,2,16,17] As each reaction sequence is limited to the number of −OH groups present on the surface, the thickness of the resulting film is determined by the number of ALD cycles. In many cases the substrate is heated to accelerate the reaction; however, near-room-temperature ALD has been reported for use with thermally unstable supports.[16,18]

Because most ALD methods require surface hydroxyl groups to be present, the preparation of the substrate surface is critical.[1,2] Although ALD growth of Al_2O_3 has been reported on noble metal surfaces and HF-etched Si, the coverage by thin (<15 nm) films of these oxides is not uniform due to poor surface nucleation.[19−21] Similarly, hydrophobic surfaces, such as methyl-terminated self-assembled monolayers (SAMs), have been shown to inhibit nucleation of AlO_x ALD films.[22] Likewise, TiO_x resists growth on alkylsilane monolayers immobilized on Si and mercaptoalkane monolayers immobilized on Au, but nucleation proceeds properly on hydroxyl-terminated alkylthiol SAMs immobilized on Au.[23,24] Studies on carbon have demonstrated that the nucleation of AlO_x ALD films starts at step edges of freshly cleaved highly oriented pyrolytic graphite (HOPG) when H_2O is used as the oxygen source. The growth of the oxide is more uniform when O_3 is used in place of H_2O.[25,26]

The ALD process is generally understood to yield continuous and conformal films one layer at a time.[8,14] As discussed above, this is not always the case, particularly on supports like carbon, Au, Pt, Pd, and Cu.[7,19,25,26] A common tool used for analysis of ALD coatings is atomic force microscopy, though it may not have sufficient resolution to reveal very small and shallow defects on rough surfaces.[23−27] In contrast, electrochemistry is

Received: August 13, 2014
Revised: October 13, 2014
Published: November 5, 2014

   dx.doi.org/10.1021/la503232m | Langmuir 2014, 30, 13707−13715

well suited for probing the size and number density of a wide range of defects within insulating thin films atop conductive substrates.[28,29] For these types of perforated, thin, insulating films, electron transfer between the electrode and an electroactive species either in solution or absorbed to the insulator can be achieved by three distinct mechanisms: (1) electron tunneling through the blocking layer,[30,31] (2) direct electron transfer at pinholes present in the insulating layer,[28,32,33] or (3) diffusion of the electroactive species through a porous network present throughout the blocking layer.[34] For example, a recent electrochemical study reported that even rather thick (>4 nm) TiO_2 ALD layers deposited onto indium tin oxide (ITO)-coated glass do not yield pinhole-free films, but rather porous deposits that exhibit microelectrode-type behavior.[35] This same study indicated that even poorer TiO_2 ALD films formed on fluorine-doped tin oxide (FTO)-coated glass, Pt, and Ag.

Most electrochemical studies making use of ALD have focused on passivation of a portion of an electrode surface, usually with Al_2O_3. Examples of this approach include electrode/nanopipet structures for scanning probe microscopy[36] and corrosion-resistant layers on steel.[37,38] Al_2O_3 ALD has also been used to passivate dye-sensitized photoelectrodes to prevent back electron transfer from a current collector to a redox shuttle.[39] Very recently, the capacitance of Al_2O_3 ALD layers prepared on ITO was reported.[40] Electrochemical methods indicated that these surfaces were pinhole-free, but due to the heterogeneous nature of the ITO surface, it was not clear whether electroinactive regions of the ITO surface, which can account for ∼99% of the total surface area, were covered with the ALD layer.[41] In the latter study, the stability of the ALD layers in the electrochemical environment was not evaluated.

Ultimately, we hope to use nanoparticle-modified ALD films on an inert electrode support as a substrate for electrocatalysis. However, prior to these studies, developing procedures to reproducibly prepare stable and defect-free films for electrochemical studies is a high priority. Therefore, in the present publication, we address some fundamental electrochemical properties of ALD films on carbon electrode supports that are required for our forthcoming catalysis studies.

EXPERIMENTAL SECTION

Chemicals and Materials. The following chemicals were used as received: KCl (>99%, Fisher Scientific, Houston, TX), KNO_3 (>99%, Fisher), K_2SO_4 (>99% Fisher), $KClO_4$ (>99%, Acros, Fair Lawn, NJ), HNO_3 (70%, ultra high purity grade, EMD Chemicals, Philadelphia, PA), HCl (37% trace metal grade, Fisher), H_2SO_4 (+95%, 99.9999% trace metal grade, Sigma-Aldrich, St. Louis, MO), and $HClO_4$ (70%, ultra pure grade, J.T. Baker, Center Valley, PA).

The ALD reagents trimethylaluminum (TMA, Sigma-Aldrich, St. Louis, MO) and tetrakis(dimethylamino)tin(IV) (TDMASn, Strem, Newburyport, MA) were obtained in sealed stainless steel canisters. Ferrocenemethanol (FcMeOH, 97%, Acros, Fair Lawn, NJ) and $AgNO_3$ (99%, Sigma-Aldrich) were used as received. High-purity N_2 (99.9999%, Praxair, Austin, TX) was used as a purge gas for the ALD process. Aqueous solutions were prepared using Milli-Q water (18.2 MΩ·cm, Millipore, Billerica, MA).

Preparation of PPF Electrodes. PPF electrodes were fabricated using a slight modification of a previously reported procedure.[5] Specifically, a positive-tone photoresist (AZ 1518, Capitol Scientific, Inc., Austin, TX) was spin-coated onto quartz slides for 45 s at 3500 rpm, soft baked for 1 min at 100 °C, and then exposed to UV light under a photomask. The exposed resist was developed using AZ 400 K developer, diluted 1/4 (v/v) with deionized water. The developed resist was then pyrolyzed in a quartz tube furnace under a forming gas consisting of 5% H_2 and 95% N_2 (Praxair) at a flow rate of 100 sccm. The temperature was ramped from 25 to 1000 °C at 5 °C/min. The temperature was held at 1000 °C for 1 h and then cooled back to 25 °C while maintaining the flow of the forming gas. The substrate was then scored with a diamond-tipped pen and broken into individual electrodes. Each electrode was rinsed with a gentle flow of deionized water and dried under N_2.

As discussed later, some PPF electrodes were treated with an air plasma (Harrick Plasma Cleaner, PDC-32G, Ithaca, NY) prior to ALD. The plasma chamber was evacuated with a roughing pump for ∼7 min, and then the substrates were exposed to the plasma at 10.5 W. The plasma-treated PPF substrates were immediately loaded into the ALD chamber for metal oxide deposition. PPF electrodes used for control experiments (not coated by ALD) were not plasma treated.

Atomic Layer Deposition. ALD was performed using a Savannah S100 Cambridge NanoTech ALD system (Ultratech, San Jose, CA). Al_2O_3 was deposited using TMA as the Al source and H_2O as the oxygen source (neither reagent was heated). The ALD system was evacuated to <1 mmHg with the walls of the chamber and the substrates heated to 150 °C under a constant flow of high-purity N_2 gas (20 sccm). After a 10 min purge with N_2, the first monolayer was deposited using the following pulse sequence, which comprises one ALD cycle: (1) a single 15 ms pulse of H_2O, (2) a 20 s purge of N_2, (3) a 15 ms pulse of TMA, and (4) a 20 s purge of N_2. This process was then repeated until the desired number of cycles was attained. SnO_2 was deposited using TDMASn as the Sn source and H_2O as the oxygen source. The H_2O was not heated, but the TDMASn was heated to 60 °C. The walls of the chamber and the substrate were heated to 150 °C under a constant flow of high-purity N_2. The system was evacuated (<1 mmHg) and purged with N_2 for 20 min prior to the deposition of the first monolayer. One ALD cycle consisted of the following pulse sequence: (1) a 15 ms pulse of H_2O, (2) a 30 s purge with N_2, (3) a 0.5 s pulse of TDMASn, and (4) a 30 s N_2 purge. This process was repeated until the desired number of ALD cycles was reached.

Surface Characterization. X-ray photoelectron spectroscopy (XPS) measurements were obtained using a Kratos Axis Ultra spectrometer (Chestnut Ridge, NY) having an Al Kα source. The PPF substrates were mounted onto the sample holder and grounded using Cu tape. An electron flood gun was used to neutralize charge on insulating substrates. Spectra of individual elements were collected with a 0.1 eV step size and a band-pass energy of 20 eV. Binding energies were calibrated against the C 1s line of the PPF (284.44 eV) substrates.[42] Peak fitting was done using CasaXPS (version 2.3.15, Casa Software, Teignmouth, UK) assuming a mixed Gaussian/Lorentzian model.

Ellipsometric measurements were obtained using a J.A. Woollam M-2000D spectroscopic ellipsometer (Lincoln, NE). Data were obtained between 300 and 900 nm using at least five different angles for each measurement. The model used to analyze the data included a thick layer of SiO_2 (1 mm) and a 300 nm thick layer of carbon. The manufacturer of the ellipsometer provided the SiO_2 optical constants required for this model, and the constants for carbon were determined experimentally using naked PPF preconditioned with air plasma. For measurements of Al_2O_3 thickness, the optical constants were provided by the manufacturer, which meant that only the thickness of the metal oxide film was allowed to float. For SnO_2, the optical constants were experimentally determined by fitting data obtained for a carbon substrate exposed to 20 ALD cycles. The initial values of the optical constants were taken from preloaded values for indium tin oxide, and then both the optical constants and the film thickness were fit. These values were held constant for the remaining SnO_2 films, allowing only for changes in thickness. The measurements were conducted in triplicate, and the linear fits were determined using a weighted linear least-squares fit.

Scanning electron microscope (SEM) micrographs were collected using a Hitachi S-5500 microscope (Dallas, TX) with a 3−5 keV electron beam at 10 μA. A Bruker energy dispersive spectroscopy (EDS) Quantex 4010 detector was used for EDS with a beam energy

dx.doi.org/10.1021/la503232m | Langmuir 2014, 30, 13707−13715

of 30 keV at 20 μA. The micrographs were processed using the ImageJ software package (NIH, Bethesda, MD).

Electrochemical Characterization. Electrochemical measurements were obtained using a CH Instruments CHI700D electrochemical analyzer (Austin, TX) and a home-built electrochemical cell. A saturated calomel reference electrode (SCE, 0.241 V v NHE, CH Instruments) and a Pt wire counter electrode were used to collect cyclic voltammograms (CVs). A silicone gasket having a 1.1 mm diameter hole was used to define the area of the working electrode. This geometric area was used to calculate current densities. In some cases, the data were smoothed using a 5-point moving average to remove instrumental noise. No *iR* compensation was used for the experiments reported herein.

Ag electrodeposition was carried out at −0.25 V vs a Hg/Hg_2SO_4 reference electrode (MSE, 0.64 V v NHE, CH Instruments) for 50 s using a solution containing 0.50 mM $AgNO_3$ and 0.10 M KNO_3. The electroactive area of the electrode was defined by a Viton O-ring to be 12.4 mm^2.

Oxygen was not removed from solutions unless specifically noted.

RESULTS AND DISCUSSION

Air-Plasma Pretreatment of PPF Electrodes. In this report, we compare ALD films deposited onto PPF films before and after exposure to an air plasma. The plasma pretreatment is intended to introduce additional oxygen functionalities to the carbon surface, which, as discussed in the Introduction, we hypothesized would improve nucleation of the oxide overlayer.

Although PPF substrates are prone to oxidation in air, the surface coverage of the oxygen-containing groups is still lower than on related carbon materials.[5,6] Figure 1a shows high-resolution C 1s XPS spectra of PPF films prior to exposure to the plasma (black trace) and after exposure for 15 s (red trace) and 30 s (blue trace). The most important feature in these spectra is a small peak (inset) fitted at 286.5−286.6 eV, which appears only after plasma treatment. We assign this peak to phenolic carbon.[43,44] A second, smaller peak also appears after plasma treatment in the 288.6−288.9 eV region of the spectra, and we assign it to carboxylic carbon.[45]

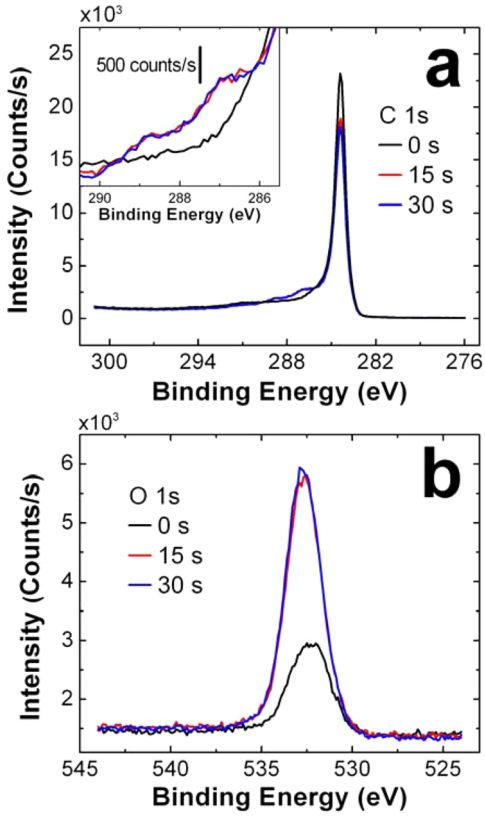

Figure 1. High-resolution XPS spectra obtained for PPF electrodes treated with an air plasma for the times indicated in the legends. Data are shown for the (a) C 1s and (b) O 1s regions. The inset in (a) shows an expanded view of the high-energy shoulder appended to the main C 1s peak.

Figure 1b shows high-resolution XPS spectra of the same substrates used to obtain the data in Figure 1a, but in this case the O 1s region is shown. The important result is that there is a substantial increase in surface O after exposure to the plasma, confirming formation of additional oxygenated species on the PPF surface.

Synthesis of ALD Layers. The method used to synthesize the ALD layers is described in the Experimental Section. As discussed there, some PPF carbon electrodes were oxidized in an air plasma to generate oxygen functional groups prior to ALD. PPFs not exposed to plasma were used as controls. The presence of the ALD films on the PPF electrodes was confirmed by XPS (Figures S1 and S2 in the Supporting Information).

Ellipsometric Measurements. The ALD process is described as a self-limiting synthesis in which at most a single monolayer of material is deposited per cycle. Therefore, a linear relationship should exist between the thickness of the metal oxide film and the number of ALD cycles. Accordingly, we deposited different numbers of Al_2O_3 and SnO_2 ALD layers onto PPF films with and without an air plasma pretreatment and measured their thicknesses using spectroscopic ellipsometry.

Figure 2a shows the measured thicknesses of Al_2O_3 ALD films on PPF electrodes before (black) and after (15 s, red; 30 s, blue) plasma pretreatment as a function of the number of ALD cycles. All these data indicate linear growth of the ALD layer, and the measured growth rates are all about the same: 0.11 ± 0.02, 0.095 ± 0.009, and 0.117 ± 0.002 nm/cycle for 0, 15, and 30 s of plasma pretreatment, respectively. The errors for the slope are generated from the weighted least-squares fit for their respective data sets. These values are comparable to the growth rate provided by the ALD system manufacturer for the deposition of Al_2O_3 onto Si(100) substrates having a native oxide layer: 0.107 nm/cycle.[46]

Figure 2b shows data analogous to that in Figure 2a, except for SnO_2 ALD films. In all cases there is linear growth of the ALD layer, though the rates are somewhat different for different times of plasma pretreatment: 0.10 ± 0.02, 0.08 ± 0.01, and 0.078 ± 0.003 nm/cycle for pretreatment times of 0, 15, and 30 s, respectively. Note that these growth rates are all slightly lower than for Al_2O_3, but significantly higher than the rate (0.053 nm/cycle) provided by the ALD system manufacturer for the deposition SnO_2 onto Si(100) substrates having a native oxide layer.[47]

For purposes of the present study, the key point about Figure 2 is that it provides calibration data that makes it possible to predict film thickness as a function of the number of ALD cycles. In subsequent subsections we will discuss the uniformity of these ALD layers as a function of their thickness.

Voltammetric Properties of PPF Electrodes Coated with Al_2O_3 ALD Films. In the future, we are interested in using ALD films for electrocatalytic studies, and therefore it is necessary to investigate their performance in typical electrochemical systems to understand the effects of substrate

dx.doi.org/10.1021/la503232m | *Langmuir* 2014, 30, 13707−13715

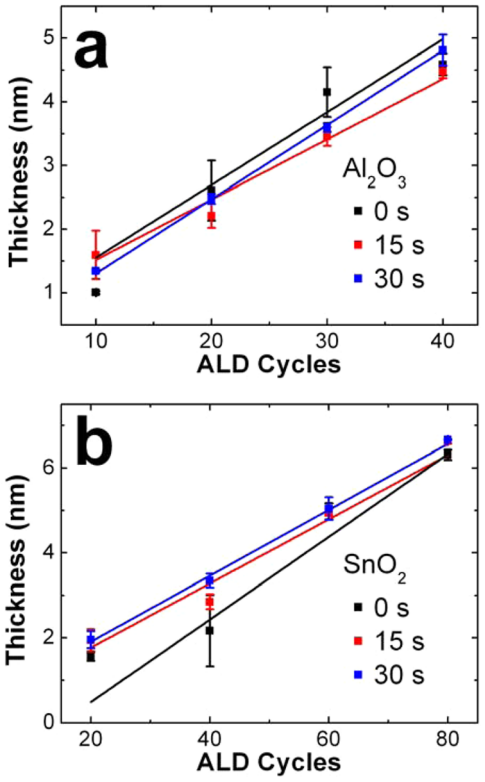

Figure 2. Thickness of the (a) Al_2O_3 and (b) SnO_2 ALD films measured by ellipsometry as a function of the plasma-treatment time (indicated in the legend) of the PPF electrodes. The error bars represent one standard deviation from the mean for three independently prepared electrodes.

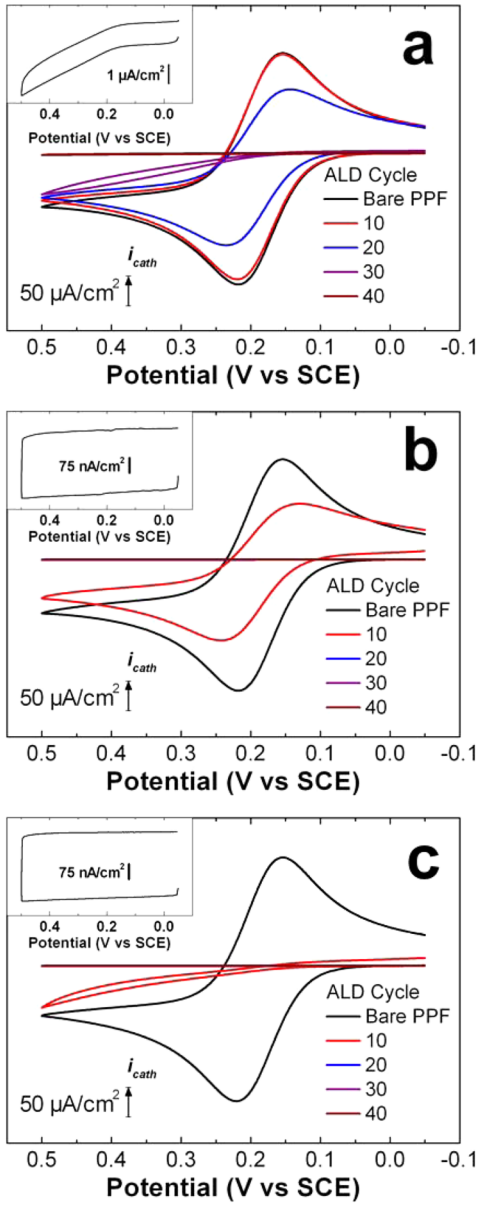

Figure 3. CVs obtained using PPF electrodes modified with the indicated number of Al_2O_3 ALD cycles. The aqueous electrolyte solution contained 1.0 mM FcMeOH and 0.10 M KNO_3. The PPF films were treated with an air plasma for the following times prior to ALD film deposition: (a) no plasma treatment; (b) 15 s; (c) 30 s. The insets show expanded views of the CVs obtained for the 40-cycle ALD films. The scan rate for each CV was 100 mV/s, and the geometric area of the PPF electrode was 0.0095 cm^2. The data in this figure were replicated two additional times: Figures S4 and S5.

pretreatment and the resulting properties of the ALD films. Accordingly, we carried out cyclic voltammetric (CV) experiments, using aqueous solutions containing 1.0 mM FcMeOH as a redox-active probe and 0.10 M KNO_3 as the supporting electrolyte, as a function of the number of ALD layers. Results for the Al_2O_3 ALD films are discussed first, followed by results for the SnO_2 films.

Figure 3a shows CVs obtained using PPF electrodes coated with 10, 20, 30, and 40 ALD cycles of Al_2O_3 but with no plasma pretreatment of the PPF surface. To ensure that the electrochemical data are representative of stable oxide films, 16 scans were obtained and only the 17th CV is presented in the figure. Here, as for all subsequent electrochemical data, the CVs are fully stable after the first two or three scans and do not change upon additional scanning. The results, as judged by the magnitude of the current density, indicate very slight passivation after 10 and 20 ALD cycles. After 40 ALD cycles, which based on ellipsometric data obtained using Figure 2a corresponds to a 4.4 ± 0.8 nm thick Al_2O_3 film, the faradaic current is greatly attenuated. However, the inset shows that oxidation of FcMeOH is still apparent at higher current resolution.

Figure 3b presents electrochemical data analogous to that in Figure 3a, except that the PPF electrode was pretreated with air plasma for 15 s prior to ALD of Al_2O_3. We hypothesized that the plasma treatment would introduce more oxygenated sites on the carbon (this was confirmed by the XPS data discussed earlier) that would in turn provide more nucleation sites for the oxide and hence more homogeneous oxide coatings. In accordance with this expectation, the decrease in faradaic current as a function of the number of ALD layers occurs much more quickly than in Figure 3a. In fact, as shown in the inset, the faradaic current arising from FcMeOH oxidation after 40 cycles of Al_2O_3, which corresponds to a calculated ellipsometric film thickness of 3.8 ± 0.4 nm, is negligible (only capacitive current is observed). Note the difference in current scales in the insets of Figures 3a and 3b.

The CVs in Figure 3c were obtained using identical conditions as in Figure 3b, but in this case the air plasma pretreatment was carried out for 30 s rather than 15 s. Here, the decrease in faradaic current is significantly faster than for the shorter plasma exposure (compare the red traces in Figures 3b

dx.doi.org/10.1021/la503232m | Langmuir 2014, 30, 13707−13715

and 3c, for example), and complete passivation is observed after 40 ALD cycles (inset, Figure 3c), corresponding to a film thickness 4.7 ± 0.7 nm.

The shape of the CVs in Figure 3 provides some qualitative hints as to the relationship between plasma pretreatment of the PPF electrodes and the structure of the resulting Al_2O_3 films. Compare, for example, the CVs corresponding to 10 ALD cycles of Al_2O_3 (red CVs in Figure 3). For ALD films deposited with no plasma pretreatment the shape of the CV is very similar to the bare PPF films: just a slight decrease in the peak anodic current ($i_{p,a}$). Compared to the data in Figure 3a, the decrease in $i_{p,a}$ is more apparent for the red CV in Figure 3b, and in addition this CV has a slightly sigmoidal appearance and the anodic peak potential ($E_{p,a}$) shifts positive by ~26 mV. These characteristics are further exaggerated for the red CV in Figure 3c. Indeed, Figure S3 shows data for three replicate measurements corresponding to the red CV to Figure 3c, but in these cases the scan limits were increased to +0.8 and −0.3 V vs. SCE so that the sigmoidal character of the CVs is more apparent.

The sigmoidal shape of the red CVs (10 ALD cycles of Al_2O_3) in Figures 3b and 3c is typical of radial diffusion to an array of small electrodes.[28,33,48−50] The preliminary conclusion is that these 10-cycle ALD films contain pinholes through which the redox probe can penetrate. It is also reasonable to surmise that as the plasma pretreatment is extended from 15 to 30 s, more nucleation sites for Al_2O_3 are introduced, and this leads to smaller and more widely spaced pinholes and hence a more clearly sigmoidal shape of the CVs. Microscopy data discussed later will confirm these preliminary observations. One final point: the CV data shown in Figure 3 are reproducible. Figures S4 and S5 in the Supporting Information are replicate electrochemical data obtained for nominally identical, but independently prepared, ALD films.

The CVs corresponding to 40 ALD cycles in Figures 3b and 3c, particularly the insets in these figures, clearly indicate the absence of pinholes. Rather, these data are characteristic of capacitive charging. Figures S6 and S7 show expanded views of the transition to this purely capacitive behavior for Al_2O_3 thin films deposited using 20, 30, and 40 ALD cycles on PPF electrodes exposed to air plasma for 15 and 30 s, respectively. Lee and co-workers have previously shown that the relationship between capacitance (C) and Al_2O_3 ALD film thickness can provide information about the electrode/ALD film/electrolyte-solution interface.[40] Specifically, a linear relationship between $1/C$ and the thickness of the ALD layer indicates that essentially all of the applied potential drops within the ALD film (rather than a fraction being dropped in the electrical double layer in solution). The average capacitances of the 20-, 30-, and 40-layer Al_2O_3 ALD films (extracted from the three sets of data in Figure S7) are 32.1, 22.6, and 15.0 nF, respectively. When the inverse of these capacitances is plotted vs film thickness, a linear correspondence is observed having an R^2 value of 0.99, indicating that most of the voltage is dropped within the oxide layer.

Voltammetric Properties of PPF Electrodes Coated with SnO_2 ALD films. SnO_2 is a reducible oxide and hence able to participate as a cocatalyst in certain electrocatalytic reactions.[51] Therefore, we are interested in understanding the behavior of thin SnO_2 ALD films, and particularly in comparing their properties to Al_2O_3, which is usually catalytically inactive. Accordingly, we carried out electrochemical experiments using SnO_2 films similar to those discussed for Al_2O_3 in the previous section.

Figure 4 is a set of CVs similar to those shown in Figure 3, but for SnO_2 ALD films. Figure 4a, for example, shows the

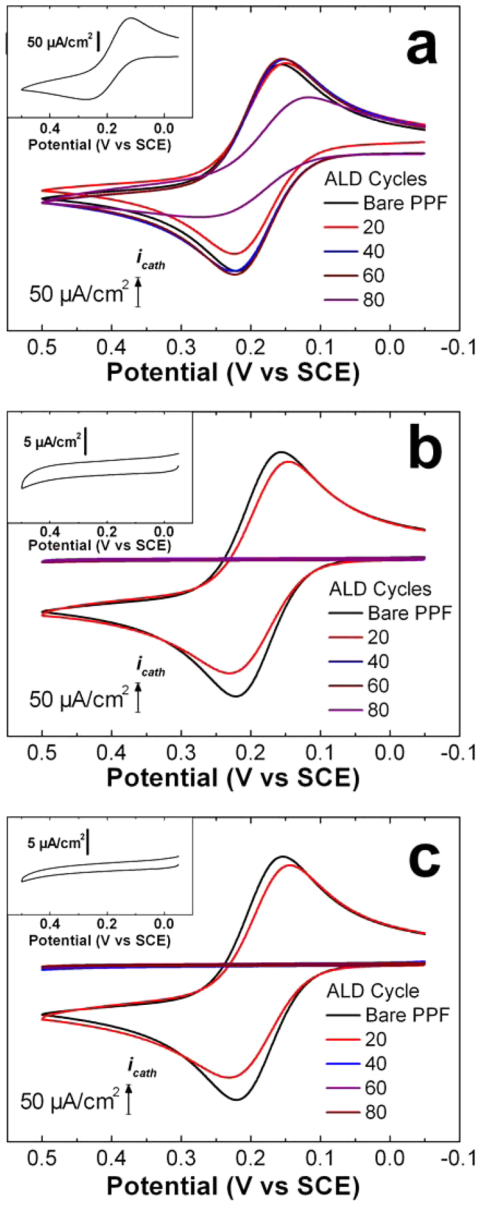

Figure 4. CVs obtained using PPF electrodes modified with the indicated number of SnO_2 ALD cycles. The aqueous electrolyte solution contained 1.0 mM FcMeOH and 0.10 M KNO_3. The PPF films were treated with an air plasma for the following times prior to ALD film deposition: (a) no plasma treatment; (b) 15 s; (c) 30 s. The insets show expanded views of the CVs obtained for the 80-cycle ALD films. The scan rate for each CV was 100 mV/s, and the geometric area of the PPF electrode was 0.0095 cm^2. The data in this figure were replicated two additional times: Figures S8 and S9.

voltammetry of FcMeOH obtained using PPF electrodes that have not been exposed to plasma treatment prior to the indicated number of SnO_2 ALD cycles. SnO_2 ALD films reportedly grow at approximately half the rate of the corresponding Al_2O_3 films, and therefore the CVs in Figure 4 were obtained using twice as many ALD cycles as for Al_2O_3.[46,47] As for the previously discussed Al_2O_3 films, the

dx.doi.org/10.1021/la503232m | Langmuir 2014, 30, 13707−13715

17th CVs are displayed. In contrast to the corresponding Al_2O_3 ALD films, however, the CVs indicate very little passivation of the PPF surface after 20, 40, and 60 ALD cycles. Even after 80 ALD cycles (inset) the decrease in faradaic current is minimal. Note that this latter film had a thickness of 8.0 ± 1 nm, which was determined using the ellipsometric calibration curve shown in Figure 2b.

Figure 4b shows electrochemical data analogous to those in Figure 4a, except the PPF substrate was treated with an air plasma for 15 s prior to ALD of SnO_2. The decrease in the faradaic current arising from FcMeOH is much faster than in Figure 4a, clearly demonstrating the importance of plasma-derived nucleation sites for SnO_2 deposition. For example, after 80 ALD cycles (inset) the faradaic current arising from FcMeOH oxidation is more than 2 orders of magnitude smaller than for films deposited on untreated PPF. The thickness of this 80-cycle film is 6.4 ± 0.8 nm.

Figure 4c shows electrochemical data analogous to those in Figures 4a and 4b, except the PPF electrodes received a 30 s air plasma pretreatment prior to ALD of SnO_2. These data are very similar to those shown in Figure 4b, indicating that the electrode surface is nearly saturated with ALD nucleation sites for SnO_2 within 15 s of plasma exposure. Note that all of the data in Figure 4 are reproducible, as evidenced by the replicate results provided in Figures S8 and S9. Also note that CVs obtained using a larger scan window for the thickest ALD film (Figure S10) reveal a rapid increase in current at potentials positive of ~0.5 V vs. SCE. This might indicate that in this case tunneling through the film is the dominant mode of electron transfer rather than direct electron transfer at pinholes.[28,30,31]

Imaging Pinholes in ALD Thin Films Using Metal Electrodeposition. We previously used a combination of electrodeposition and microscopy to visualize pinholes in self-assembled alkylthiol monolayers.[57] In this approach, a metal, such as Ag or Cu, is selectively deposited only at electroactive defect sites within an otherwise insulating thin film. In effect, this amplifies the size of the defects and makes it possible to image the number of defects and their spatial distribution. We adopt this same general approach here to better understand the nature of defects in SnO_2 and Al_2O_3 ALD films as a function of film thickness.

In the present study the defect size in the oxide films was amplified using Ag electrodeposition, and then the resulting metal islands were imaged using scanning electron microscopy (SEM). Figure 5a is a representative micrograph of Ag electrodeposited onto PPF electrode pretreated with 15 s of air plasma followed by 10 Al_2O_3 ALD cycles. Ag electrodeposition was carried out by immersing the ALD-coated PPF electrode in a solution containing 0.50 mM $AgNO_3$ and 0.10 M KNO_3 and then stepping the potential to a sufficiently negative potential (−0.25 V vs. MSE) for 50 s to deposit Ag. The identity of the light-colored islands in Figure 5a was determined using EDS, which indicated the presence of Ag (Figure S11d). In contrast, no Ag was observed in the dark regions of the surface (e.g., on the pinhole-free regions of the oxide). The size of the Ag islands is typically on the order of ~1 μm (Figure 5c), but this is not a direct reflection of the defect size, which is surely much smaller. In other words, the Ag electrodeposition method is useful for approximating the number of defects that penetrate through the ALD film, but not for judging their absolute size.

Figure 5b was obtained under the same conditions as for Figure 5a, but in this case the PPF electrode was treated with plasma for 30 s, rather than 15 s, prior to coating with 10 ALD cycles of Al_2O_3. Both the size and number of Ag islands are smaller in this case. As noted in the previous paragraph, the size of the Ag islands does not reflect the absolute size of the underlying defects, but the relative sizes of the islands may correlate to relative defect size. The island number density was estimated using at least 10 randomly selected micrographs from each of two independently prepared PPF electrodes. The results indicate an average density of (3.1 ± 2) × 10^6 and (1.4 ± 1) × 10^6 islands per cm^2 for 15 and 30 s plasma pretreatments, respectively. This corresponds to about 1−3 islands per 100 μm^2. Similar measurements were conducted on PPF films (15 and 30 s plasma treatment times) coated with 20 ALD cycles of SnO_2, and the corresponding number density of islands was found to be (1.5 ± 0.2) × 10^6 and (1.5 ± 1.0) × 10^6 Ag islands per cm^2, respectively (Figures S11a and S11b).

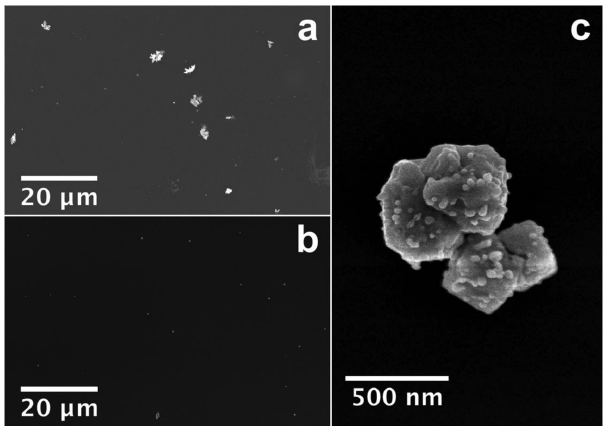

Figure 5. Representative SEM micrographs of Ag electrodeposited onto PPF films coated with Al_2O_3 (10 ALD cycles). In (a) the PPF film was treated with an air plasma for 15 s prior to ALD. For (b) the plasma time was 30 s. (c) An enlarged view of a typical Ag island deposited onto a substrate prepared as in (b).

The trend in the pinhole concentrations correlates with the trend from the electrochemical measurements. In the Al_2O_3 films we observed that the rate of passivation increases with the amount of plasma treatment for 10 cycles of Al_2O_3 (see the red CVs in Figures 3b and 3c). This corresponds to more of the underlying PPF electrode being covered with Al_2O_3 and thus a lower pinhole concentration. In contrast, the CVs corresponding to the substrates exposed to 20 cycles of SnO_2 ALD after 15 and 30 s of plasma pretreatment (red CVs in Figures 4b and 4c) are similar, indicating that the surface coverage of SnO_2 is approximately the same. This is consistent with the identical pinhole densities measured using the Ag electrodeposition method.

Stability of ALD Films in Other Electrolytes. In the future, we plan to use these ALD films as substrates for electrocatalytic reactions in acidic solutions, and therefore we examined their stability at low pH. Figure S12 shows CVs obtained in a solution containing 1.0 mM FcMeOH and 0.10 M $HClO_4$ using a PPF electrode pretreated with 30 s of air plasma and then coated with 40 ALD cycles of Al_2O_3. Even after 17 consecutive CVs, only a slight faradaic current (tens of nA/cm^2 compared to >100 $\mu A/cm^2$ on the bare PPF electrode) arising from FcMeOH is observed. Figure S13 provides CVs under the same conditions, but in this case FeMeOH was omitted. The results reveal a much lower (and stable) capacitive current for the ALD-coated electrode.[40] We conclude

dx.doi.org/10.1021/la503232m | Langmuir 2014, 30, 13707−13715

that these very thin Al_2O_3 layers are stable in acidic electrolytes. Also note that the capacitance of the Al_2O_3 films is approximately the same regardless of whether FcMeOH is present in solution.

In addition to determining the stability of the Al_2O_3 films in $HClO_4$ solutions, we also examined stability in several other common electrolytes (0.10 M) using 1.0 mM FcMeOH as the redox probe. Figure S14 shows the first and tenth CVs of oxidized PPF electrodes (15 s air plasma) coated with 30 ALD cycles of Al_2O_3. As judged by the current density arising from FcMeOH oxidation, the Al_2O_3 films are stable on the 10 CV time scale (~20 min) in KNO_3, K_2SO_4, KCl, $KClO_4$, and HNO_3, but not HCl or H_2SO_4. This outcome is not too surprising, because Al_2O_3 is known to be soluble in acidic solutions having complexing ligands.[58] Experiments analogous to those just discussed for Al_2O_3 were carried out using electrodes coated using 100 ALD cycles of SnO_2 (Figure S15). These films were stable in all eight of the electrolytes examined.

SUMMARY AND CONCLUSIONS

Here we have shown that carbon PPF electrodes can be modified with thin, passivating layers of Al_2O_3 and SnO_2 deposited via ALD. A key finding is that less defective films result when oxygen functionalities are introduced onto the carbon surface prior to ALD. This is presumably because oxygenation leads to a higher surface density of ALD nucleation sites. ALD films of Al_2O_3 just ~3−4 nm in thickness result in complete passivation of the PPF surface toward faradaic electrochemical reactions. The SnO_2 films are not as passivating as Al_2O_3, but coatings of ~6 nm in thickness block faradaic current. Importantly, both the Al_2O_3 and SnO_2 films are stable in many neutral and acidic common electrolytes even after repeated voltammetric scanning.

It has recently been shown that passivating films having thicknesses on the same order as those reported here can be rendered electrochemically active if metal nanoparticles are immobilized on their surface.[59,60] This finding provides a basis for using thin ALD oxide films as substrates for nanoparticle-catalyzed electrochemical reactions.[51,61] We are presently carrying out such studies, and the results will be published in due course.

ASSOCIATED CONTENT

Supporting Information

XPS of the PPF electrodes and the ALD films, CVs having extended potential windows, CVs having expanded current scales, replicate CV experiments, SEM micrographs, EDS spectra, and evaluation of the stability of the ALD films in different electrolytes. This material is available free of charge via the Internet at http://pubs.acs.org.

AUTHOR INFORMATION

Corresponding Author

*E-mail: crooks@cm.utexas.edu (R.M.C.).

Notes

The authors declare no competing financial interest.

ACKNOWLEDGMENTS

We gratefully acknowledge support from the Chemical Sciences, Geosciences, and Biosciences Division, Office of Basic Energy Sciences, Office of Science, U. S. Department of Energy (Contract DE-FG02-13ER16428). R.M.C. thanks the Robert A. Welch Foundation (Grant F-0032) for sustained support. We thank the Surface Analysis Laboratory at the Texas Materials Institute and the National Science Foundation (Grant No. 0618242) for funding the Kratos Axis Ultra XPS used in this work. We are grateful to Dr. Hugo Celio for his assistance with the XPS measurements. We acknowledge the Center for Nano- and Molecular Science at The University of Texas at Austin for use of the ellipsometer. We also thank Dr. Abdou K. Diallo for his assistance in the early stages of this project.

REFERENCES

(1) George, S. M. Atomic Layer Deposition: An Overview. *Chem. Rev.* **2010**, *110*, 111−131.
(2) Puurunen, R. L. Surface Chemistry of Atomic Layer Deposition: A Case Study for the Trimethylaluminum/Water Process. *J. Appl. Phys.* **2005**, *97*, 121301.
(3) Peng, Q.; Lewis, J. S.; Hoertz, P. G.; Glass, J. T.; Parsons, G. N. Atomic Layer Deposition for Electrochemical Energy Generation and Storage Systems. *J. Vac. Sci. Technol., A* **2012**, *30*, 010803.
(4) Detavernier, C.; Dendooven, J.; Pulinthanathu Sree, S.; Ludwig, K. F.; Martens, J. A. Tailoring Nanoporous Materials by Atomic Layer Deposition. *Chem. Soc. Rev.* **2011**, *40*, 5242−5253.
(5) Dumitrescu, I.; Yancey, D. F.; Crooks, R. M. Dual-Electrode Microfluidic Cell for Characterizing Electrocatalysts. *Lab Chip* **2012**, *12*, 986−993.
(6) Ranganathan, S.; McCreery, R. L. Electroanalytical Performance of Carbon Films with near-Atomic Flatness. *Anal. Chem.* **2001**, *73*, 893−900.
(7) Lu, J.; Elam, J. W.; Stair, P. C. Synthesis and Stabilization of Supported Metal Catalysts by Atomic Layer Deposition. *Acc. Chem. Res.* **2013**, *46*, 1806−1815.
(8) Parsons, G. N.; George, S. M.; Knez, M. Progress and Future Directions for Atomic Layer Deposition and ALD-Based Chemistry. In *MRS Bulletin*; Materials Research Society: Warrendale, PA, 2011; pp 865−871.
(9) Marichy, C.; Bechelany, M.; Pinna, N. Atomic Layer Deposition of Nanostructured Materials for Energy and Environmental Applications. *Adv. Mater.* **2012**, *24*, 1017−1032.
(10) Aleskovskii, V. B. Chemistry and Technology of Solids. *Zh. Prikl. Khim.* **1974**, *47*, 2145−2157.
(11) Sun, L.; Thomas, R. C.; Crooks, R. M.; Ricco, A. J. Real-Time Analysis of Chemical Reactions Occurring at a Surface-Confined Organic Monolayer. *J. Am. Chem. Soc.* **1991**, *113*, 8550−8552.
(12) Kim, Y.-G.; Crooks, R. M. Synthesis and Characterization of Covalently Linked Multilayer Films Prepared in the Absence of Solvent. *Langmuir* **2005**, *21*, 11262−11267.
(13) Leskelä, M.; Ritala, M. Atomic Layer Deposition Chemistry: Recent Developments and Future Challenges. *Angew. Chem., Int. Ed.* **2003**, *42*, 5548−5554.
(14) Baker, L.; Cavanagh, A. S.; Yin, J.; George, S. M.; Kongkanand, A.; Wagner, F. T. Growth of Continuous and Ultrathin Platinum Films on Tungsten Adhesion Layers Using Atomic Layer Deposition Techniques. *Appl. Phys. Lett.* **2012**, *101*, 111601.
(15) Elam, J. W.; Zinovev, A. V. V; Pellin, M. J.; Comstock, D. J.; Hersam, M. C. Nucleation and Growth of Noble Metals on Oxide Surfaces Using Atomic Layer Deposition. *ECS Trans.* **2007**, *3*, 271−278.
(16) Heo, J.; Hock, A. S.; Gordon, R. G. Low Temperature Atomic Layer Deposition of Tin Oxide. *Chem. Mater.* **2010**, *22*, 4964−4973.
(17) Dillon, A. C.; Ott, A. W.; Way, J. D.; George, S. M. Surface Chemistry of Al_2O_3 Deposition Using $Al(CH_3)_3$ and H_2O in a Binary Reaction Sequence. *Surf. Sci.* **1995**, *322*, 230−242.
(18) Groner, M. D.; Fabreguette, F. H.; Elam, J. W.; George, S. M. Low-Temperature Al_2O_3 Atomic Layer Deposition. *Chem. Mater.* **2004**, *16*, 639−645.
(19) Groner, M. D.; Elam, J. W.; Fabreguette, F. H.; George, S. M. Electrical Characterization of Thin Al_2O_3 Films Grown by Atomic

Layer Deposition on Silicon and Various Metal Substrates. *Thin Solid Films* **2002**, *413*, 186−197.
(20) Besling, W. F. A.; Young, E.; Conard, T.; Zhao, C.; Carter, R.; Vandervorst, W.; Caymax, M.; De Gendt, S.; Heyns, M.; Maes, J.; Tuominen, M.; Haukka, S. Characterisation of ALCVD Al_2O_3−ZrO_2 Nanolaminates, Link between Electrical and Structural Properties. *J. Non-Cryst. Solids* **2002**, *303*, 123−133.
(21) Copel, M.; Gribelyuk, M.; Gusev, E. Structure and Stability of Ultrathin Zirconium Oxide Layers on Si(001). *Appl. Phys. Lett.* **2000**, *76*, 436−438.
(22) Kobayashi, N. P.; Donley, C. L.; Wang, S.-Y.; Williams, R. S. Atomic Layer Deposition of Aluminum Oxide on Hydrophobic and Hydrophilic Surfaces. *J. Cryst. Growth* **2007**, *299*, 218−222.
(23) Seo, E. K.; Lee, J. W.; Sung-Suh, H. M.; Sung, M. M. Atomic Layer Deposition of Titanium Oxide on Self-Assembled-Monolayer-Coated Gold. *Chem. Mater.* **2004**, *16*, 1878−1883.
(24) Park, M. H.; Jang, Y. J.; Sung-Suh, H. M.; Sung, M. M. Selective Atomic Layer Deposition of Titanium Oxide on Patterned Self-Assembled Monolayers Formed by Microcontact Printing. *Langmuir* **2004**, *20*, 2257−2260.
(25) Speck, F.; Ostler, M.; Röhrl, J.; Emtsev, K. V.; Hundhausen, M.; Ley, L.; Seyller, T. Atomic Layer Deposited Aluminum Oxide Films on Graphite and Graphene Studied by XPS and AFM. *Phys. Status Solidi C* **2010**, *7*, 398−401.
(26) Lee, B.; Park, S.-Y.; Kim, H.-C.; Cho, K.; Vogel, E. M.; Kim, M. J.; Wallace, R. M.; Kim, J. Conformal Al_2O_3 Dielectric Layer Deposited by Atomic Layer Deposition for Graphene-Based Nanoelectronics. *Appl. Phys. Lett.* **2008**, *92*, 203102.
(27) Garces, N. Y.; Wheeler, V. D.; Hite, J. K.; Jernigan, G. G.; Tedesco, J. L.; Nepal, N.; Eddy, C. R., Jr.; Gaskill, D. K. Epitaxial Graphene Surface Preparation for Atomic Layer Deposition of Al_2O_3. *J. Appl. Phys.* **2011**, *109*, 124304.
(28) Amatore, C.; Savéant, J. M.; Tessier, D. Charge Transfer at Partially Blocked Surfaces: A Model for the Case of Microscopic Active and Inactive Sites. *J. Electroanal. Chem. Interfacial Electrochem.* **1983**, *147*, 39−51.
(29) Amatore, C.; Savéant, J. M.; Tessier, D. Kinetics of Electron Transfer to Organic Molecules at Solid Electrodes in Organic Media. *J. Electroanal. Chem. Interfacial Electrochem.* **1983**, *146*, 37−45.
(30) Bard, A. J.; Faulkner, L. R. *Electrochemical Methods: Fundamentals and Applications*; Wiley: New York, 2001; pp 619−628.
(31) Becka, A. M.; Miller, C. J. Electrochemistry at ω-Hydroxy Thiol Coated Electrodes. 3. Voltage Independence of the Electron Tunneling Barrier and Measurements of Redox Kinetics at Large Overpotentials. *J. Phys. Chem.* **1992**, *96*, 2657−2668.
(32) Gueshi, T.; Tokuda, K.; Matsuda, H. Voltammetry at Partially Covered Electrodes: Part I. Chronopotentiometry and Chronoamperometry at Model Electrodes. *J. Electroanal. Chem. Interfacial Electrochem.* **1978**, *89*, 247−260.
(33) Gueshi, T.; Tokuda, K.; Matsuda, H. Voltammetry at Partially Covered Electrodes: Part Ii. Linear Potential Sweep and Cyclic Voltammetry. *J. Electroanal. Chem. Interfacial Electrochem.* **1979**, *101*, 29−38.
(34) Leddy, J.; Bard, A. J. Polymer Films on Electrodes: Part XII. Chronoamperometric and Rotating Disk Electrode Determination of the Mechanism of Mass Transport through Poly(Vinyl Ferrocene) Films. *J. Electroanal. Chem. Interfacial Electrochem.* **1983**, *153*, 223−242.
(35) Satpati, A. K.; Arroyo-Currás, N.; Ji, L.; Yu, E. T.; Bard, A. J. Electrochemical Monitoring of TiO_2 Atomic Layer Deposition by Chronoamperometry and Scanning Electrochemical Microscopy. *Chem. Mater.* **2013**, *25*, 4165−4172.
(36) Comstock, D. J.; Elam, J. W.; Pellin, M. J.; Hersam, M. C. Integrated Ultramicroelectrode−Nanopipet Probe for Concurrent Scanning Electrochemical Microscopy and Scanning Ion Conductance Microscopy. *Anal. Chem.* **2010**, *82*, 1270−1276.
(37) Díaz, B.; Światowska, J.; Maurice, V.; Seyeux, A.; Normand, B.; Härkönen, E.; Ritala, M.; Marcus, P. Electrochemical and Time-of-Flight Secondary Ion Mass Spectrometry Analysis of Ultra-Thin Metal Oxide (Al_2O_3 and Ta_2O_5) Coatings Deposited by Atomic Layer Deposition on Stainless Steel. *Electrochim. Acta* **2011**, *56*, 10516−10523.
(38) Díaz, B.; Härkönen, E.; Maurice, V.; Światowska, J.; Seyeux, A.; Ritala, M.; Marcus, P. Failure Mechanism of Thin Al_2O_3 Coatings Grown by Atomic Layer Deposition for Corrosion Protection of Carbon Steel. *Electrochim. Acta* **2011**, *56*, 9609−9618.
(39) Hamann, T. W.; Farha, O. K.; Hupp, J. T. Outer-Sphere Redox Couples as Shuttles in Dye-Sensitized Solar Cells. Performance Enhancement Based on Photoelectrode Modification Via Atomic Layer Deposition. *J. Phys. Chem. C* **2008**, *112*, 19756−19764.
(40) Lee, H.; Chang, B.-Y.; Kwack, W.-S.; Jo, K.; Jeong, J.; Kwon, S.-H.; Yang, H. Dependence of the Capacitance between an Electrode and an Electrolyte Solution on the Thickness of Aluminum Oxide Layers Deposited Using Atomic Layer Deposition. *J. Electroanal. Chem.* **2013**, *700*, 8−11.
(41) Armstrong, N. R.; Veneman, P. A.; Ratcliff, E.; Placencia, D.; Brumbach, M. Oxide Contacts in Organic Photovoltaics: Characterization and Control of Near-Surface Composition in Indium−Tin Oxide (Ito) Electrodes. *Acc. Chem. Res.* **2009**, *42*, 1748−1757.
(42) NIST X-Ray Photoelectron Spectroscopy Database, Version 4.1; National Institute of Standards and Technology, Gaithersburg, MD, 2012; http://srdata.nist.gov/xps/.
(43) Jones, C.; Sammann, E. The Effect of Low Power Plasmas on Carbon Fibre Surfaces: A Comparison between Low and High Modulus PAN Based Fibres with Pitch Based Carbon Fibres. *Carbon* **1990**, *28*, 515−519.
(44) Cabaniss, G. E.; Diamantis, A. A.; Murphy, W. R., Jr.; Linton, R. W.; Meyer, T. J. Electrocatalysis of Proton-Coupled Electron-Transfer Reactions at Glassy Carbon Electrodes. *J. Am. Chem. Soc.* **1985**, *107*, 1845−1853.
(45) Moulder, J. F.; Stickle, W. F.; Sobol, P. E.; Bomben, K. D. *Handbook of X-Ray Photoelectron Spectroscopy*; Physical Electronics USA, Inc.: Chanhassen, MN, 1995.
(46) Al_2O_3 - Aluminum Oxide Savannah Film Recipe; R083011; Cambridge Nanotech Inc., Waltham, MA, 2011.
(47) SnO_2 - Tin Dioxide Savannah Film Recipe; R090711; Cambridge Nanotech Inc., Waltham, MA, 2011.
(48) Finklea, H. O.; Snider, D. A.; Fedyk, J.; Sabatani, E.; Gafni, Y.; Rubinstein, I. Characterization of Octadecanethiol-Coated Gold Electrodes as Microarray Electrodes by Cyclic Voltammetry and ac Impedance Spectroscopy. *Langmuir* **1993**, *9*, 3660−3667.
(49) Chailapakul, O.; Crooks, R. M. Synthesis and Characterization of Simple Self-Assembling, Nanoporous Monolayer Assemblies: A New Strategy for Molecular Recognition. *Langmuir* **1993**, *9*, 884−888.
(50) Chailapakul, O.; Crooks, R. M. Interactions between Organized, Surface-Confined Monolayers and Liquid-Phase Probe Molecules. 4. Synthesis and Characterization of Nanoporous Molecular Assemblies: Mechanism of Probe Penetration. *Langmuir* **1995**, *11*, 1329−1340.
(51) Zhou, W.-P.; Axnanda, S.; White, M. G.; Adzic, R. R.; Hrbek, J. Enhancement in Ethanol Electrooxidation by SnO_x Nanoislands Grown on Pt(111): Effect of Metal Oxide−Metal Interface Sites. *J. Phys. Chem. C* **2011**, *115*, 16467−16473.
(52) Smart, L.; Moore, E. *Solid State Chemistry: An Introduction*, 3rd ed.; CRC Press: Boca Raton, FL, 2005.
(53) Halim, A. Thin Films Made from Colloidal Antimony Tin Oxide Nanoparticles for Transparent Conductive Applications. In *School of Materials Science and Engineering*; Georgia Insitute of Technology: Atlanta, GA, 2013; p 23.
(54) Fortunato, E.; Barquinha, P.; Martins, R. Oxide Semiconductor Thin-Film Transistors: A Review of Recent Advances. *Adv. Mater.* **2012**, *24*, 2945−2986.
(55) Noufi, R. N.; Kohl, P. A.; Frank, S. N.; Bard, A. J. Semiconductor Electrodes XIV. Electrochemistry and Electroluminescence at N-Type TiO_2 in Aqueous Solutions. *J. Electrochem. Soc.* **1978**, *125*, 246−252.
(56) Schmitt, S. W.; Gamez, G.; Sivakov, V.; Schubert, M.; Christiansen, S. H.; Michler, J. Chemical and Optical Characterisation of Atomic Layer Deposition Aluminium Doped Zno Films for

Photovoltaics by Glow Discharge Optical Emission Spectrometry. *J. Anal. At. Spectrom.* **2011**, *26*, 822−827.
(57) Sun, L.; Crooks, R. M. Imaging of Defects Contained within N-Alkylthiol Monolayers by Combination of Underpotential Deposition and Scanning Tunneling Microscopy: Kinetics of Self-Assembly. *J. Electrochem. Soc.* **1991**, *138*, L23−L25.
(58) Deltombe, E.; Vanleugenhaghe, C.; Pourbaix, M. Aluminium. In *Atlas of Electrochemical Equilibria in Aqueous Solutions*; Pourbaix, M., Ed.; Pergamon Press: New York, 1966; pp 168−176.
(59) Chazalviel, J.-N.; Allongue, P. On the Origin of the Efficient Nanoparticle Mediated Electron Transfer across a Self-Assembled Monolayer. *J. Am. Chem. Soc.* **2010**, *133*, 762−764.
(60) Kissling, G. P.; Miles, D. O.; Fermín, D. J. Electrochemical Charge Transfer Mediated by Metal Nanoparticles and Quantum Dots. *Phys. Chem. Chem. Phys.* **2011**, *13*, 21175−21185.
(61) Zhou, W.-P.; An, W.; Su, D.; Palomino, R.; Liu, P.; White, M. G.; Adzic, R. R. Electrooxidation of Methanol at SnOx−Pt Interface: A Tunable Activity of Tin Oxide Nanoparticles. *J. Phys. Chem. Lett.* **2012**, *3*, 3286−3290.